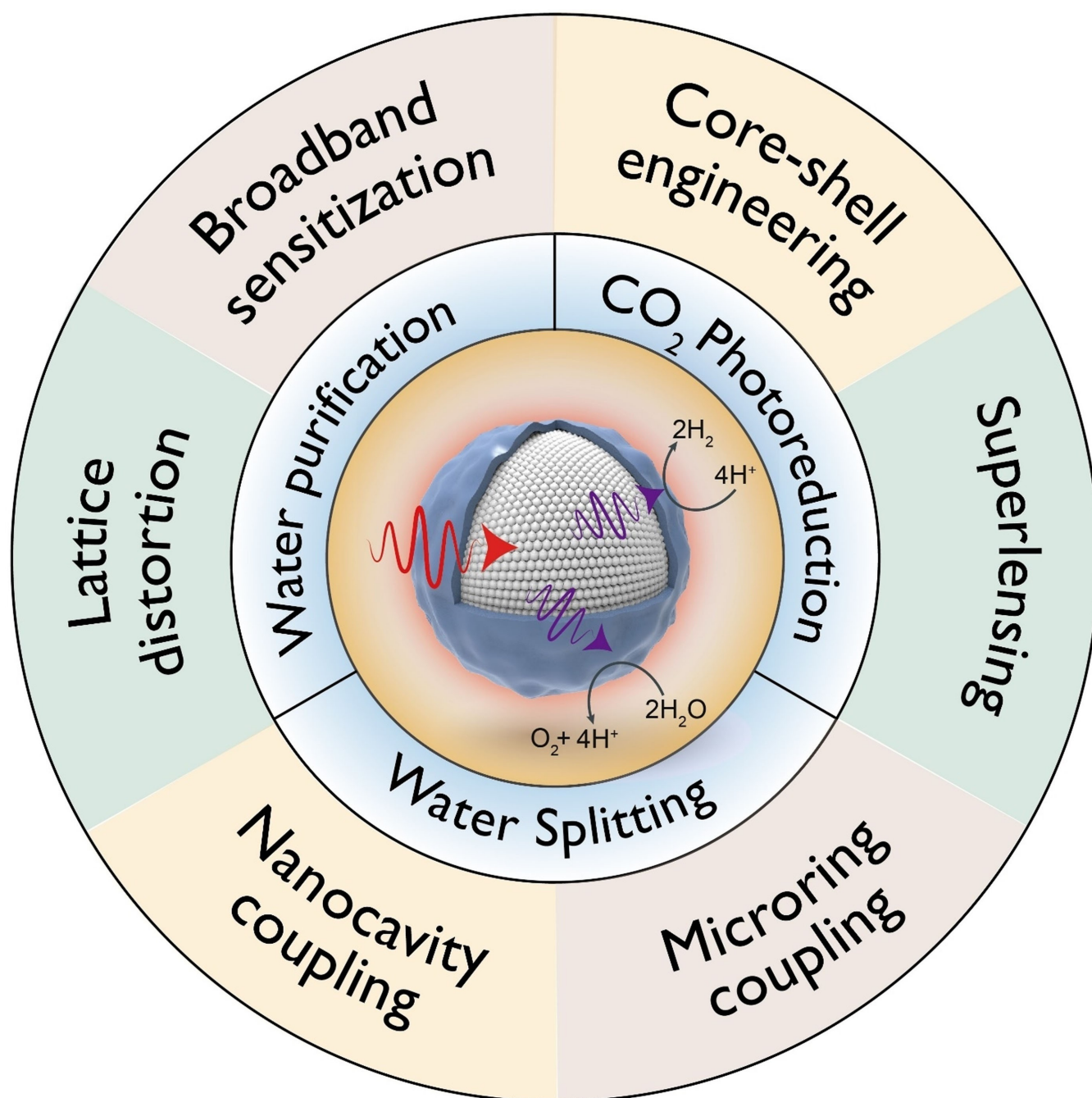Special Collection

Multiphoton Upconversion Materials for Photocatalysis and Environmental Remediation

Yiming Wu,*[a] Siew Yin Chan,[a] Jiahui Xu,[b] and Xiaogang Liu*[a, b]

Abstract: Solar-driven photocatalysis holds great potential for energy conversion, environmental remediation, and sustainable chemistry. However, practical applications of conventional photocatalytic systems have been constrained by their insufficient ability to harvest solar radiation in the infrared spectrum. Lanthanide-doped upconversion materials possess high photostability, tunable absorption, and the ability to convert low-energy infrared radiation into high-energy emission, making them attractive for infrared-driven photo-catalysis. This review highlights essential principles for rational design of efficient photocatalysts. Particular emphasis is placed on current state-of-the-arts that offer enhanced upconversion luminescence efficiency. We also summarize recent advances in lanthanide-doped upconversion materials for photocatalysis. We conclude with new challenges and prospects for future developments of infrared-driven photo-catalysts.

1. Introduction

As energy crisis and environmental pollution have become an increasingly global concern, the development of renewable and clean energy resources via environmentally friendly technologies has become a matter of urgency. Solar energy has gained considerable research interest as a clean, sustainable energy source. As a direct photon-to-chemical conversion technology, photocatalysis utilizes inexhaustible solar energy or artificial light sources to degrade pollutants and produce storable chemical fuels (Figure 1a), representing an economic and sustainable route to potentially tackle the environmental pollution and energy crisis.[1–3] In this regard, it is imperative to develop efficient photocatalysts capable of harvesting the broad solar spectrum with improved photocatalytic efficiency.

Numerous semiconductors with high photocatalytic reactivity were synthesized in recent decades, such as SnO_2, ZnO, and TiO_2.[4–8] Under solar irradiation, photocatalytic semiconductors can activate chemical transformations. In general, photocatalysis is a multistep process comprising three main sequential processes (Figure 1b).[9–11] In the first step, electrons in a semiconductor are excited to the conduction band by absorbing solar photons with energy equal or larger than the semiconductor bandgap, generating electron-hole pairs with excited electrons in the conduction band and holes in the valence band. These electrons and holes then diffuse to semiconductor surfaces separately. Finally, diffused electrons and holes participate in photoreduction and photooxidation, respectively. The efficiencies of these three processes thus decide the overall solar-to-chemical conversion efficiency of a photocatalytic reaction. Wide-bandgap semiconductors, such as TiO_2, have been extensively investigated in various photocatalytic reactions due to their high reactivity, cost-effectiveness, and environmental sustainability.[12] Since the discovery of

TiO_2 photocatalysis in 1972, many other semiconductors with wide bandgaps, such as BiOCl and ZnO, have shown excellent UV-driven photocatalytic properties.[13–15] However, the absorption threshold of these materials is typically in the UV region (300–400 nm) because of their bandgaps of ~3.0 eV, which covers only 6% of the full solar spectrum and restricts full utilization of solar photons. Moreover, energy losses exist both in the visible (44%, 400–700 nm) and NIR (50%, 700–2500 nm) region, limiting solar conversion efficiency.[16] Alternatively, semiconductors with narrower bandgaps (CdS, Fe_2O_3, and g-C_3N_4) can be developed to extend the absorption threshold to the visible spectrum in order to improve photocatalytic efficiency (Figure 2).[17–20] In addition, surface functionalization of wide-bandgap semiconductors has proven effective in harvesting wide-spectral solar energy.[21,22]

Although visible-driven photocatalytic systems exhibit improved sunlight harvesting, solar energy utilization efficiency is still limited because ultraviolet (UV) and visible light only account for 50% of the solar spectrum. To improve photocatalytic efficiency for industrial applications, it is critical to develop practical strategies for harvesting the remaining 50% of infrared light. Lanthanide-based upconversion nanoparticles (UCNPs) are promising candidates as infrared-driven photocatalytic systems because of their unique nonlinear optical property, namely the ability to convert near-infrared (NIR) light into UV or visible emission (Figure 1c).[23–25] Upconverted photons can be utilized by most semiconductor photocatalysts. In addition, UCNPs exhibit tunable absorption in the infrared region, extending solar harvesting to a broader spectral range. These features have made UCNPs promising for photocatalytic and photovoltaic applications. In recent years, tremendous research efforts have been made to increase the NIR responsivity of semiconductor photocatalysts by combining upconversion materials.[26–29] This review highlights recent achievements in NIR-driven photocatalysis involving lanthanide-doped UCNPs. We start with a brief introduction to basic design principles for semiconductor photocatalysts. Particular emphasis is placed on upconversion luminescence enhancement, which is essential for the future design of efficient photocatalysts with broadband absorption in the NIR region. Furthermore, we present a collection of specific examples that showcase the broad utility of upconversion materials for photocatalysis. We conclude with prospects and challenges related to the future development of NIR-driven photocatalysts.

[a] Dr. Y. Wu, Dr. S. Y. Chan, Prof. X. Liu
Institute of Materials Research and Engineering
Agency for Science, Technology and Research
Singapore 138634 (Singapore)
E-mail: wu_yiming@imre.a-star.edu.sg

[b] Dr. J. Xu, Prof. X. Liu
Department of Chemistry
National University of Singapore
Institution 3 Science Drive 3, Singapore 117543 (Singapore)
E-mail: chmlx@nus.edu.sg

Special Collection This manuscript is part of a Special Collection on Metals in Functional Materials and Catalysis.

Yiming Wu obtained his B.Eng. degree (2010) in Material Science and Engineering from Changshu Institute of Technology, China. He received his M.S. degree (2013) in Inorganic Chemistry from Soochow University and completed his Ph.D. (2018) in the group of Professor Xiaogang Liu at the National University of Singapore. He then carried out postdoctoral work at the National University of Singapore for three years. He is currently a scientist in the Institute of Materials Research and Engineering (IMRE), Agency for Science, Technology and Research (A*STAR), Singapore. His current research interest lies in the rational design of frequency conversion nanomaterials for optoelectronic applications.

Siew Yin Chan received her BSc in Food Science and Technology with First Class Honours (2013) and subsequently obtained her Ph.D. in Chemical Science (2018) from Monash University. She is currently a scientist in the Institute of Materials and Engineering (IMRE), Agency for Science, Technology and Research (A*STAR), Singapore. She was previously an Assistant Professor in the Institute of Flexible Electronics at Northwestern Polytechnical University, China. Her research interests focus on sustainable functional materials and green solutions for plastic management.

Jiahui Xu received her B.S. (2014) degree in Chemistry from Soochow University, P.R. China. She earned her M.S. (2015) and Ph.D. (2020) degrees from National University of Singapore under the direction of Professor Xiaogang Liu. She is currently a postdoctoral researcher in the Department of Electrical and Computer, Engineering, NUS. Her research interests focus on lanthanide-doped luminescent nanomaterials and light-matter interaction in nanophotonic structures.

Xiaogang Liu received his B.E. degree in Chemical Engineering from Beijing Technology and Business University, China. He received his M.S. degree in Chemistry from East Carolina University and completed his Ph.D. at Northwestern University. He then carried out postdoctoral work at MIT for two years before joining the National University of Singapore in 2006. Currently, he sits as an Associate Editor for Nanoscale. His research encompasses areas including nanostructured catalysis, optical nanomaterials, optogenetic neuromodulation, and X-ray imaging.

2. Fundamental Principles of Semiconductor Photocatalysts

2.1. Working Principle of Photocatalysis

Photocatalysis mimics nature's photosynthesis, enabling solar energy to be transformed into chemical fuels. During this process, photoactive materials absorb photons with energies equal to or larger than their bandgaps to yield electron-hole pairs, which can subsequentially support photoreaction processes. The redox potentials of these charge carriers are determined by the band positions of photoactive catalysts. In general, the rate of both exergonic and endergonic reactions can be promoted with the aid of solar energy (Figure 3).[30] The photoexcitation was found to reduce the kinetic barrier of exergonic reactions, such as dye degradation, which are thermodynamically spontaneous ($\Delta G < 0$) irrespective of the light absorption. On the contrary, for an endergonic reaction to proceed ($\Delta G > 0$), high-energy photons are normally required to participate in the reaction. Water splitting is a typical example of such a reaction.

2.2. Strategies for Designing Efficient Photocatalysts

Semiconductors with high catalytic properties often exhibit wide bandgaps and require UV light for efficient excitation. Harvesting solar energy using wide bandgap semiconductors remains challenging. Thus far, numerous techniques have been successfully developed to tailor the band structure of photocatalytic semiconductors in an attempt to extend the absorption range for broadband photocatalysis. In the following section, different strategies for enhancing photocatalytic systems are highlighted.

2.2.1. Doping and defect engineering

Introducing foreign elements into the crystal lattice of a photocatalytic semiconductor host represents an efficient strategy for bandgap engineering.[31–33] In principle, metal doping and defect engineering are beneficial for the generation of intermediate states due to the interaction between cation states and conduction bands or valence bands (Figure 4a). This strategy has been widely employed to extend the absorption of wide-bandgap semiconductor photocatalysts to the visible range. The redshifted absorption edge of $SrTiO_3$ exemplified this effectiveness through co-doping with Ni^{2+}/Ta^{5+}, Cr^{3+}/Sb^{5+}, or Cr^{3+}/Ta^{5+}.[34–36] In such cases, the electron donor level is generated above the valence band of $SrTiO_3$ by doping metal cations into the host matrix, forming a new energy gap matching the visible range. Structural defects can be used to modulate the electronic structure and charge carrier dynamics of photocatalysts.[37,38] A notable example is catalytically active BiOBr with deliberately created oxygen vacancies that provide interband states for visible absorption.[39] In addition, enrich-

a

b

c
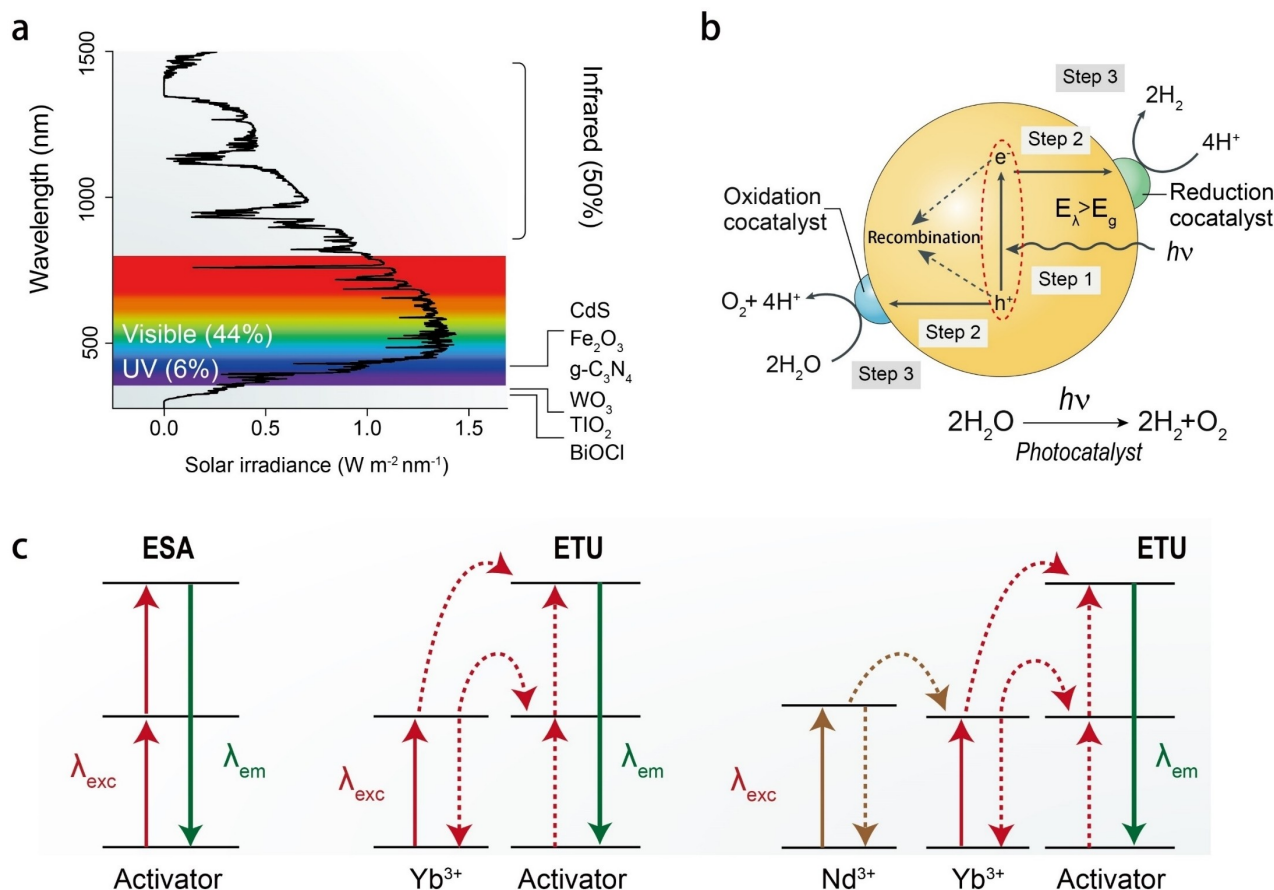
Figure 1. (a) The majority of the solar spectrum. The UV, visible and NIR regions constitute 6%, 44% and 50% of the full spectrum, respectively. (b) Schematics of the main processes within the overall photocatalytic water-splitting reaction. E_λ and E_g are the energy of the incident photon and the semiconductor bandgap, respectively. (c) Schematics showing three efficient upconversion pathways for NIR harvesting. ESA and ETU represent excited state absorption and energy transfer upconversion. (a) Reproduced with permission from Ref. [16], Copyright 2018, Springer Nature. (b) Reproduced with permission from Ref. [9], Copyright 2017, Springer Nature.
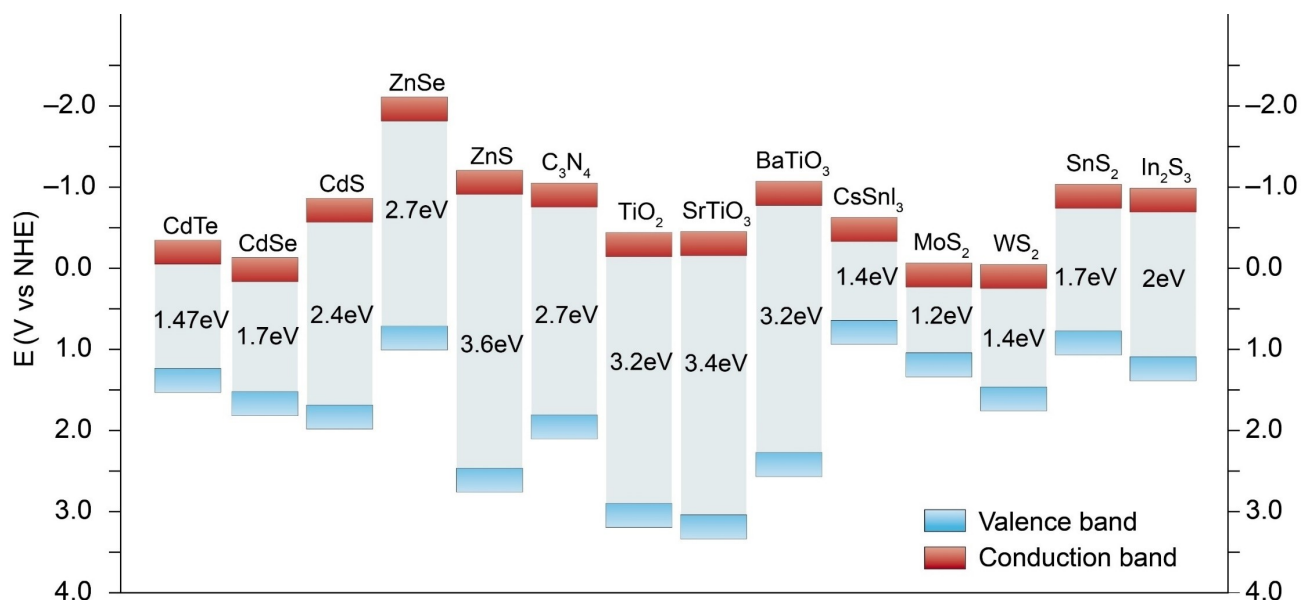
Figure 2. Bandgap energies of widely investigated photocatalytic semiconductors. Reproduced with permission from Ref. [16], Copyright 2018, Springer Nature.

a

b

c Photoinduced reduction

down-hill

d Photo energy conversion reaction

up-hill
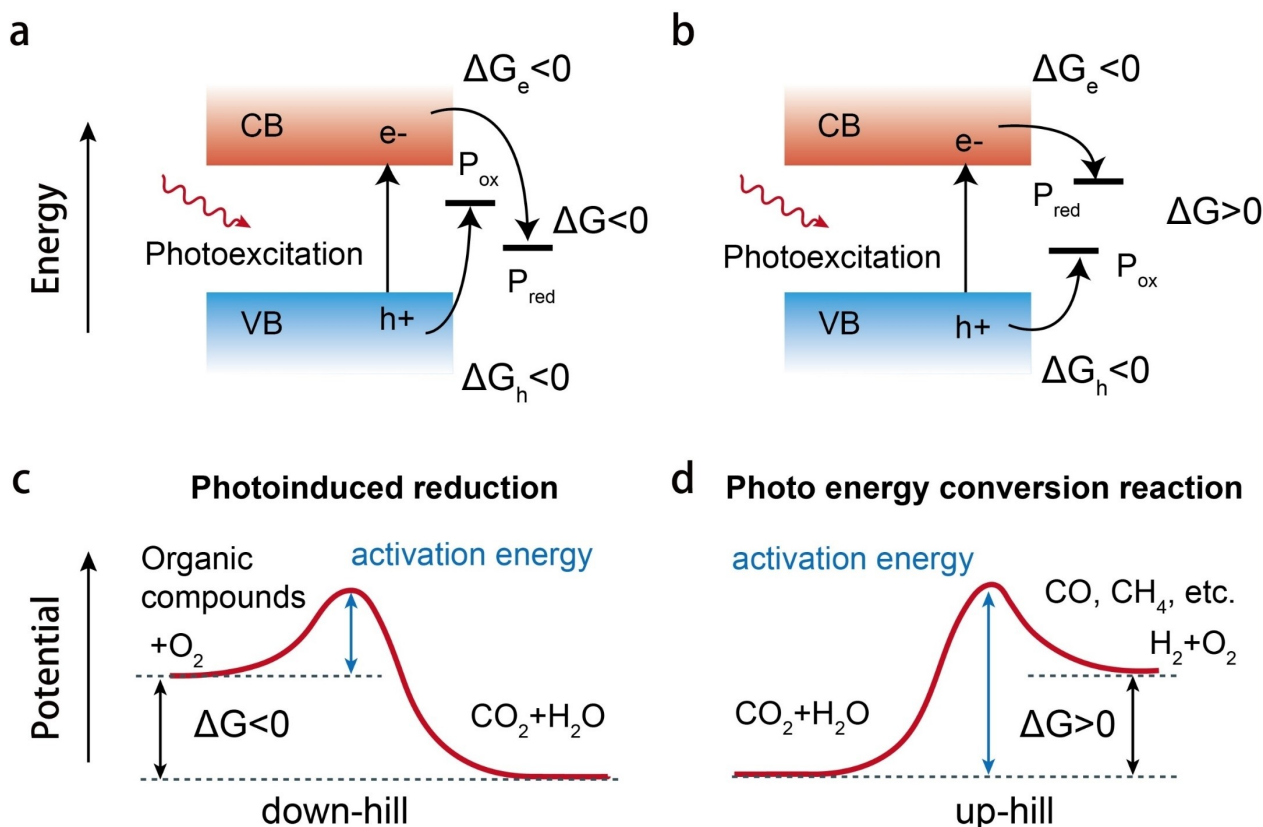
Figure 3. (a, b) Electronic structure of photocatalytic semiconductors. ΔG is the change in Gibbs free energy. P_{ox} is the oxidation potential of the reactant to be oxidized. P_{red} is the reduction potential of the reactant to be reduced. (c) Gibbs energy change ($\Delta G < 0$) in downhill photocatalytic reactions such as photocatalytic degradation. (d) Gibbs energy change ($\Delta G > 0$) in downhill photocatalytic reactions such as photosynthesis and artificial photosynthesis. (a–d) Reproduced with permission from Ref. [30]. Copyright 2017, Royal Society of Chemistry.

ment of the zinc vacancy also improves charge separation and carrier transfer in 3D hierarchical $ZnIn_2S_4$.[40]

2.2.2. VB potential engineering

Incorporating transition metals into semiconductors is another efficacious approach to develop visible-driven photocatalysts because transition metal ions can promote band formation above the valence band comprising O 2p orbitals in different hosts (Figure 4b). For instance, metal cations and anions with filled s or d orbitals, such as Cu^+, Ag^+, Sn^{2+}, Pb^{2+} and Bi^{3+}, have been applied to the construction of valence bands with more negative potentials than O 2p orbitals in oxide oxyhalides, (oxy) sulfides, and (oxy)nitrides.[41–46] These technology developments ultimately lead to narrower semiconductor bandgaps and thus improved solar energy utilization.

2.2.3. Solid solution synthesis

Another approach to modulating the optical properties of photocatalysts is to form a solid solution of different isostructural semiconductors (Figure 4c). Orbitally hybridized atoms and distorted metal-oxygen structural units of the mixture can change band structures.[47–50] In addition, by varying the proportions of wide- and narrow-bandgap semiconductors, the bandgaps and energy levels of these materials can be precisely adjusted, offering an effective and flexible way to design efficient visible-driven photocatalysts.

2.2.4. Dye-sensitization

Functionalization of semiconductor photocatalysts with light-harvesting organic molecules offers a versatile solution to reduce effective bandgaps, enabling photocatalytic reactions under NIR irradiation (Figure 4d). Active molecules with suitable lowest unoccupied molecular orbital (LUMO) and highest occupied molecular orbital (HOMO) energy levels have been introduced to redshift the absorption onset.[51–54] Upon excitation, generated electrons inject into the conduction band and then contribute to reduction reactions.

2.2.5. Surface plasmon resonance (SPR)

Sensitization of wide-bandgap semiconductors with metallic nanoparticles via surface plasmon resonance has great potential to assist semiconductor photocatalysts in harvesting low-energy
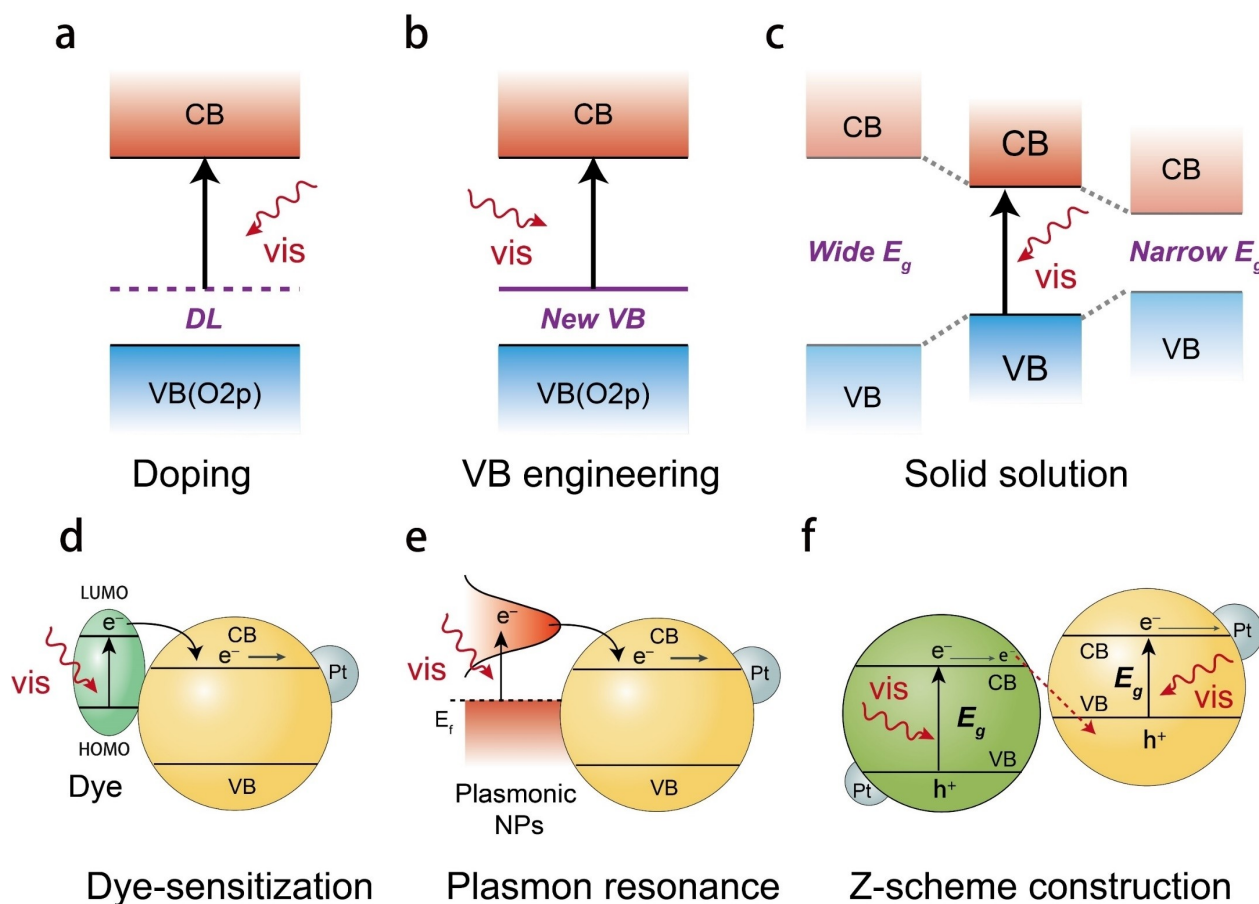
Figure 4. Schematics showing strategies for narrowing the bandgap of photocatalysts with broadband absorption in visible light through (a) doping and defect engineering, (b) valence band engineering, (c) solid solution formation, (d) dye-sensitization, (e) surface plasmon resonance coupling, and f) Z-scheme construction. (a–f) Reproduced with permission from Ref. [4], Copyright 2019, American Chemical Society.

photons.[55,56] Metallic gold (Au) and silver (Ag) nanoparticles display intense SPR, with extinction coefficients several orders of magnitude higher than those of typical dye molecules.[57] Plasmonic nanoparticles resonating with incident light at specific frequencies can generate hot carriers that being sequentially transferred to closely contacted photocatalysts, participating in specific photocatalytic reactions (Figure 4e). Moreover, by adjusting the size, shape and composition of nanoparticles, plasmonic resonant frequency can be tuned in a wide spectral range from the visible to the NIR region,[58–60] providing a flexible strategy to modifying photocatalytic absorption.

2.2.6. Z-scheme configuration

The Z-scheme system relies on a two-photon absorption process in a hybrid structure that comprises two materials with different bandgaps (Figure 4f).[61–63] Under visible irradiation, electron-hole pairs are generated in both of the photocatalytic components. In addition, narrow bandgaps in a Z-scheme system generally exhibit a relatively larger absorption range in the solar spectrum, which is particularly useful for photo-

catalysis because of its effectiveness in capturing sunlight and enhancing charge carrier separation.

3. Strategies to Harvest NIR Photons

Coupling photocatalysts with nonlinear optical materials has become an increasingly appealing method to improve solar energy utilization in photocatalysis by harvesting NIR light. Nonlinear optical phenomena of frequency upconversion mainly include multiphoton absorption in fluorescent molecules and nanocrystals, second harmonic generation (SHG) in non-linear crystals, triplet-triplet annihilation (TTA), and photon upconversion in lanthanide-doped nanoparticles.[64–67] Of special interest are lanthanide-based upconversion materials, with the ability to sequentially absorb two or more low-energy photons and convert them into emission at shorter wavelengths. Compared with SHG or multiphoton absorption, photon upconversion in lanthanide-doped particles bypasses high-power coherent excitation and stringent phase matching, enabling an efficiency of 10^6-fold greater than conventional multiphoton absorption processes.[68] Although TTA systems exhibit large absorption cross-sections and high upconversion

efficiencies, they usually suffer from relatively small anti-Stokes shifts and poor stability in aqueous and oxygen environments.[69] In contrast, lanthanide-doped UCNPs offer sharp multi-peak line emissions, large anti-Stokes shifts, excellent photostability, and zero-autofluorescence interference,[70–72] making lanthanide-activated upconversion attractive for numerous applications.[73–77]

The photophysics of lanthanide-activated energy upconversion is primarily determined by long-lived, ladder-like energy levels of trivalent rare-earth ions, originating from $4f^n$ orbital splitting due to Coulombic interaction and spin-orbit coupling.[78] Thus, modulation of lanthanide dopants in UCNPs permits two- to six-photon upconversion processes that support significant anti-Stokes shifts to the UV-vis spectral region upon NIR irradiation. Upconverted emissions could be reabsorbed by surrounding photocatalytic materials via fluorescent resonance energy transfer. In this way, UCNPs act as optical energy nanoantennas to indirectly utilize NIR light for photocatalysis.

4. Strategies for Enhancing Upconversion Luminescence

To improve NIR photocatalysis in diverse photocatalytic systems, efficient photon absorption and upconversion are essential. Over the past decades, tremendous research efforts have been devoted to the development of efficient UCNPs. This section discusses state-of-the-art strategies for improving the brightness of upconversion emission, mainly including host-lattice manipulation, dopant concentration variation, core-shell structure engineering, local electromagnetic field modulation, and broadband sensitization.

4.1. Host-lattice Manipulation

Upconversion nanocrystals consist of an inorganic host embedded with sensitizer and activator ions. Their conversion efficiencies are closely related to the crystal structure, host phonon energy, and local site symmetry.[79] Doping lanthanide ions into a host matrix with low phonon energy presents a straightforward method to improve upconversion luminescence efficiency. Low-phonon-energy hosts prohibit quenching of radiative emission due to minimized nonradiative energy loss (Figure 5d).[80] Currently, fluoride and oxide host materials with low phonon energies and excellent chemical stability are commonly utilized for achieving efficient upconversion.[81–83] Despite having low lattice phonon energy, halides have limited applications for photon upconversion because of their hygroscopic nature.

4.2. Host Lattice Distortion

In principle, electric dipole transitions in lanthanide ions are forbidden by the parity selection rule.[84] However, lowering the crystal-field symmetry of lanthanides by crystal lattice modification can mitigate this quantum mechanical constraint and greatly increase optical transition probability, thereby intensifying upconversion luminescence (Figure 5b). This concept was well exemplified in lithium-doped oxide or fluoride hosts, which led to the distortion of local site symmetry around lanthanide emitters and enhanced upconversion luminescence.[85] Similarly, introducing transition-metal ions, such as Zn^{2+}, Bi^{3+}, Fe^{3+} and Sc^{3+}, into lanthanide-doped oxide and fluoride hosts can also boost upconversion emission.[86–89]
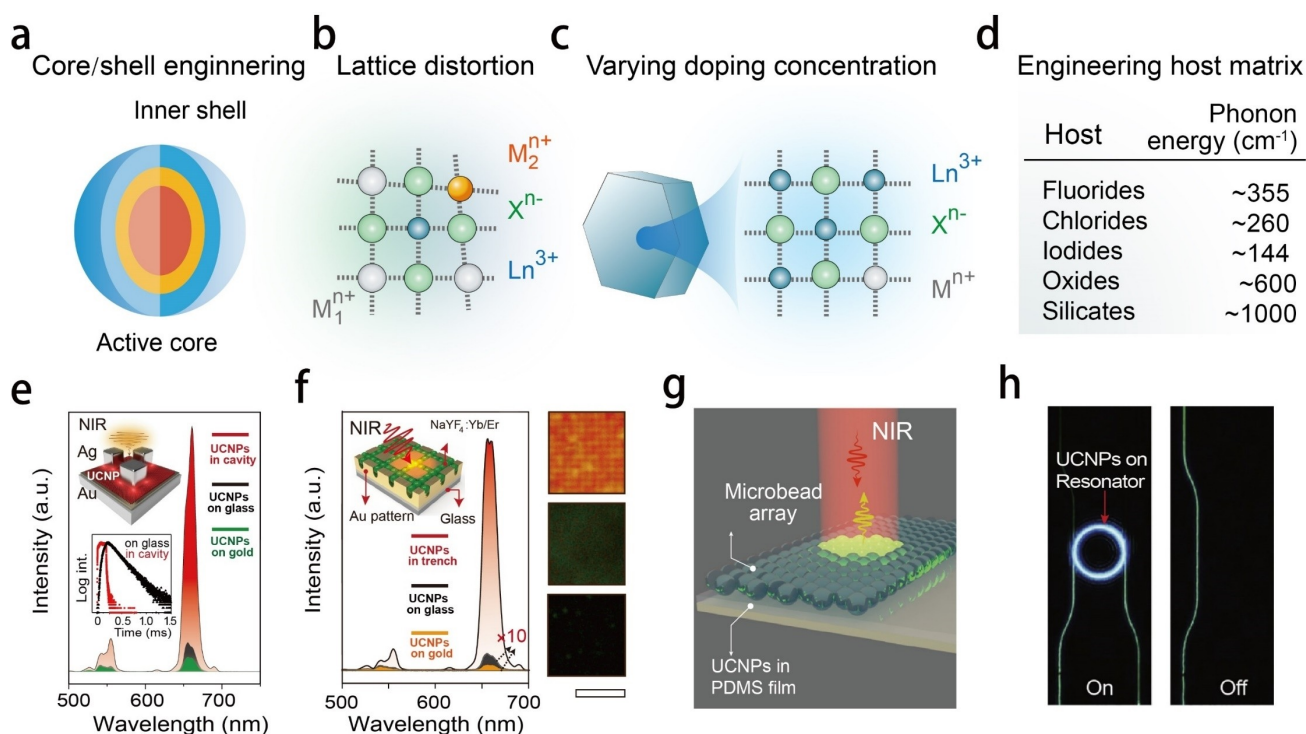
4.3. Dopant Concentration Variation

Another straightforward method to increase upconversion efficiency is to elevate doping levels of both sensitizers and activators (Figure 5c). However, lanthanide ions must be kept stringently at relatively low concentrations. A doping level exceeding the typical threshold value (~ 2 mol% for Er^{3+} or Tm^{3+}) can cause marked quenching of upconversion luminescence due to an increased probability in energy migration to surface defects or deleterious cross-relaxation between two neighboring activators.[90] Great efforts have been made to overcome concentration quenching in luminescent nanoparticles. For example, orthorhombic KYb_2F_7:Er (2 mol%) nanocrystals were developed for photon upconversion, despite a high Yb^{3+} content of 98 mol%.[91] In that study, Yb^{3+} ions were arranged in discrete tetrad atomic clusters. Trapping excitation energy in isolated sublattices effectively minimized excitation energy migration, greatly enhancing four-photon violet upconversion emission at 410 nm. In another study on α-NaYF$_4$: Er(10 mol%)@NaYbF$_4$@NaYF$_4$ nanoparticles, Zhou and co-workers proposed a multilayered structure design to alleviate the detrimental quenching effect.[92] Researchers discovered that cross-relaxation can be suppressed by spatial confinement of sensitizers and activators in neighboring layers, enabling high-efficiency energy transfer upconversion at the interface. As a result, the multilayered structure with a high doping level enhanced multiphoton emission from Er^{3+} by 100-fold.

4.4. Core-Shell Structure Engineering

Compared with their bulky counterparts, lanthanide-doped UCNPs often suffer from much stronger surface quenching owing to their high surface-to-volume ratios.[93] The luminescence of the surface dopants can be readily quenched by surface defects, ligands, and solvent molecules through multiphonon relaxation processes. Surface passivation by conformal coating of an epitaxial layer onto nanoparticles has become a routine practice to suppress the surface-dopant-induced quenching of excitation energy (Figure 5a).[94] A typical example was demonstrated in multilayered α-NaYF$_4$:Er (10 mol%)

Figure 5. Schematic strategies for enhancing upconversion emission through (a) core-shell engineering, (b) lattice distortion, (c) dopant concentration variation, (d) host matrix manipulation, (e, f) plasmonic nanocavity coupling, (g) dielectric microbead coupling, and (h) microring resonator coupling. Notably, (e) depicts photoluminescence spectra of a UCNP monolayer deposited on a glass substrate (black) and a gold film (green) or in the nanocavity (red). Insets show the comparison of decay time for UCNPs deposited on a glass substrate (black) and in the nanocavity mode (red) at an emission wavelength of 660 nm and the schematic of the gap plasmon-UCNP system. (f) shows the upconversion luminescence spectra and corresponding luminescence images of UCNPs assembled within gold nanotrenches (top), on a glass slide (middle), and on an unpatterned gold film (bottom). Scale bar: 3 μm. (g) is the schematic of the superlens setup. A layer of UCNPs is placed under an array of microbeads. (h) are micrographs of a UCNP-coated microring waveguide in on- and off-resonance states. (e) Reproduced with permission from Ref. [99], Copyright 2019, Springer Nature; (f) Reproduced with permission from Ref. [100], Copyright 2021, American Chemical Society. (g) Reproduced with permission from Ref. [103], Copyright 2019, Springer Nature; (h) Reproduced with permission from Ref. [104], Copyright 2019, Springer Nature;

@NaYbF$_4$@NaYF$_4$ UCNPs.[92] Through the core-shell design, both activators and sensitizers were spatially confined in separated layers. The Yb^{3+}-doped active shell protects the core from nonradiative decay and facilitates the transfer of absorbed NIR photons to the core. Moreover, the interior core with a relatively high doping concentration of Er^{3+} activators is beneficial for minimizing the back transfer process of excited energy, leading to a high quantum yield (6.34%). In another representative demonstration, Chen et al. designed and synthesized NaYF$_4$:Yb/Tm@NaYbF$_4$@NaYF$_4$ core-multi-shell nanoparticles, which showed ~240 times and ~11 times brightness than those well-investigated NaYF$_4$:Yb/Tm and NaYF$_4$:Yb/Tm@NaYF$_4$ nanoparticles.[95] Thus far, the rational design of core-shell structures has enabled a universal, efficient way to develop bright UCNPs for various applications.

4.5. Local Electromagnetic Field Modulation

Metallic nanostructures capable of supporting localized surface plasmon resonance have been extensively applied to improving the luminescence efficiency of UCNPs.[96,97] The resonance modes of plasmonic structures can be precisely tailored by tuning their morphologies and compositions. Among various nanostructures, metallic nanogaps with ultrasmall mode volumes have attracted much interest because of their ability to generate electromagnetic hot spots of high field intensity, providing a promising route to enhancing upconversion luminescence.[98] Recently, gap plasmon modes were used to mitigate the inherently forbidden transition of lanthanides and achieve ultrabright, fast and highly directional upconversion emission. The designed nanoresonators consist of a silver nanocube-coupled gold mirror structure with a nanoscale gap filled with UCNPs (Figure 5e). Strong nanocavity-UCNP coupling led to an over 10,000-fold enhanced emission intensity and a 166-fold increased emission rate.[99] Based on a similar strategy, Xu et al. demonstrated significantly intensified upconversion luminescence by coupling UCNPs to metallic nanotrenches.[100] A bottom-up self-assembly technique was used to realize site-specific integration of UCNPs within sub-25 nm gold nanotrenches (Figure 5f). Such metallic nanostructures confined incident light into a deep-subwavelength photonic hotspot with a maximum field enhancement ($|E/E_0|$) of 50, giving rise to significantly enhanced photon flux of excitation.

As with plasmonic counterparties, dielectric materials can generate strong electric and magnetic resonance modes by

manipulating the wavefront of excitation light.[101,102] Liang et al. demonstrated that coupling UCNPs to dielectric microbeads can remarkably improve the absorption of excitation light and thus significantly enhance upconversion processes in lanthanide-doped nanocrystals (Figure 5g).[103] As a nonlinear effect, upconverted emission intensity is proportional to the nth power of the pumping power density, where 'n' represents the number of photons required to populate the activator. Dielectric microbeads can confine an incident beam of light into a sub-wavelength photonic hotspot with high local excitation power. Although the output power of the laser source remains unchanged, UCNPs behind dielectric microbeads can probe a much higher pumping photon flux. As a result, significantly enhanced upconversion processes can be realized under low-power excitation by harnessing the dielectric superlens effect. By placing a layer of $NaGdF_4$:Yb/Tm@$NaGdF_4$:Eu nanoparticles behind an array of dielectric microbeads, luminescence can be amplified by five orders of magnitude for 614 nm emission of Eu^{3+} ($^5D_0 \rightarrow {}^7F_2$ transition) under 980 nm excitation at 1.5 Wcm^{-2}. Another example by Wang et al. demonstrated that by applying $NaErF_4$@$NaYF_4$ UCNPs on the surface of a high-index doped silica-based microring resonator (Figure 5h), intense UV emission at 380 nm with over 5% quantum yield can be achieved under 1550 nm excitation.[104]

4.6. Broadband Sensitization

Functionalization of UCNPs with organic molecules or quantum dots has become a popular strategy to improving upconversion efficiency.[105,106] These photosensitizers exhibit broad absorption bands and extinction coefficients orders of magnitude higher than those of lanthanide sensitizers. In that regard, the absorption cross-section of lanthanide sensitizers can be principally enhanced by coupling UCNPs with NIR-absorbing dyes or quantum dots. Tethered NIR dyes harvest NIR excitation and transfer it to lanthanides via Föster or Dexter energy transfer mechanisms (Figure 6a).[107] In addition, organic dyes radiatively decay much faster than lanthanide-doped UCNPs with inherently forbidden optical transitions. Organic dye-sensitization can significantly increase the radiative emission rates of lanthanide emitters.

Numerous NIR dyes with emission bands overlapping the absorption spectra of lanthanide sensitizers have been exploited as photosensitizers for UCNPs. Recent investigations
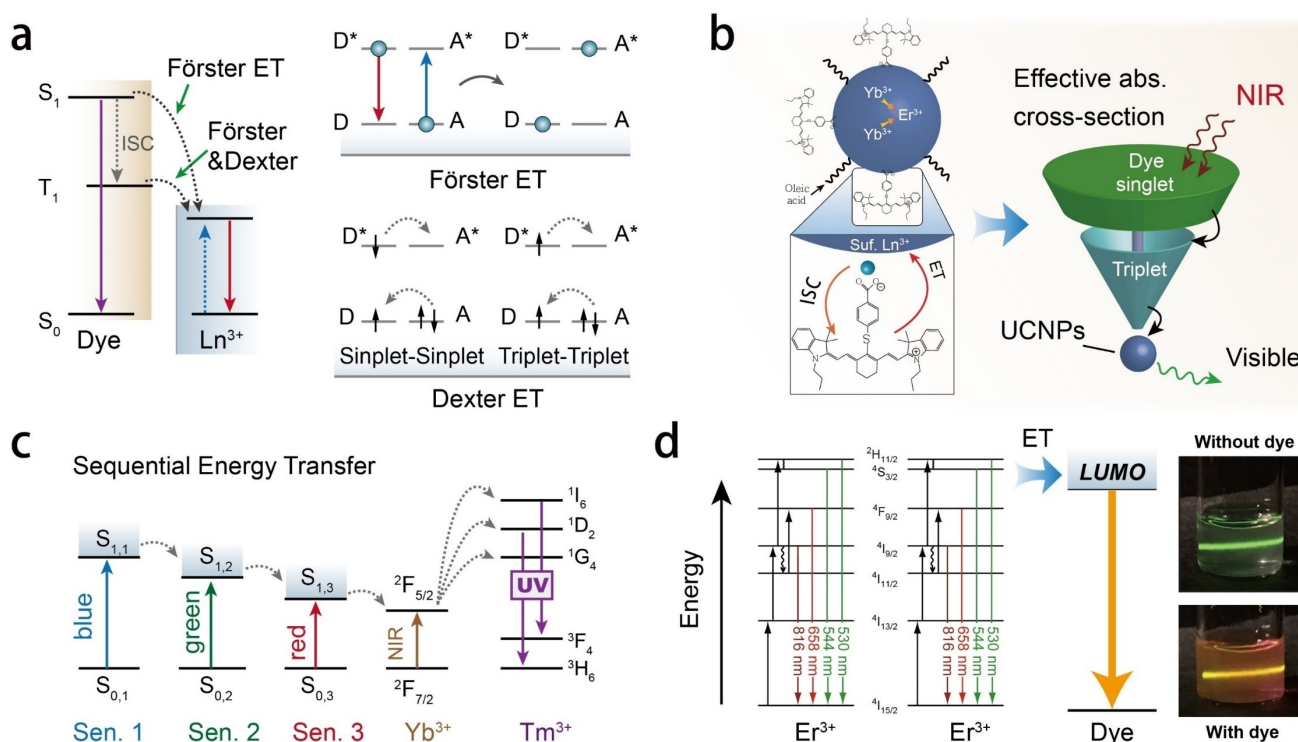
Figure 6. (a) Schematics of nonradiative energy transfer (ET) processes from the dye to lanthanide ions through Förster and Dexter mechanisms. ISC represents the intersystem crossing. (b) Schematic showing the IR-806 dye-sensitized UCNP system. NIR dyes strongly harvest NIR light and then transfer it to lanthanide ions. Increasing lanthanide contents with heavy nuclei leads to more efficient intersystem crossing from IR-806 S^1 to T^1 states due to the heavy atom effect. Enrichment of the molecular antenna triplets can significantly increase the brightness of UCNPs. (c) Multi-dye-sensitized $NaYF_4$:Yb/Tm nanoparticles exhibit dramatically widen absorption from the NIR to the entire visible range through sequential energy transfer, resulting in intensified upconverted blue emission. (d) Schematic summarizing the concept of emission dye-sensitization. UCNPs are decorated with fluorescent dye ATTO-542 having a much faster radiative decay rate. The LUMO level of ATTO-542 molecules is aligned with the $^2H_{11/2}$ and $^4S_{3/2}$ states in Er^{3+} (left), enabling efficient energy transfer from Er^{3+} to dye molecules. Micrographs of dye-sensitized (top right) and non-sensitized UCNPs in aqueous conditions (bottom right). (b) Reproduced with permission from Ref. [109], Copyright 2018, Springer Nature; (c) Reproduced with permission from Ref. [110], Copyright 2017, Wiley-VCH; (d) Reproduced with permission from Ref. [111], Copyright 2018, American Chemical Society.

have shown that sensitization of UCNPs by singlet or triplet states of NIR dye molecules can improve upconversion luminescence thousands of times. In 2015, Prasad et al. introduced the concept of cascade energy UC and showed that dye-sensitization of NaYbF$_4$:Tm@NaYF$_4$:Nd core-shell nanoparticles using IR-808 NIR dye was able to obtain a high upconversion quantum yield of ~4.8% under 800 nm excitation at 10 Wcm^{-2}.[108] Most recently, an innovative study by Garfield et al. demonstrated that the brightness and stability of the dye-UCNP systems are critically influenced by molecular triplet states (Figure 6b).[109] The heavy atom effect dramatically enhanced intersystem crossing (ISC) within dye molecules, resulting in efficient production of triplet states. Enrichment of molecular antenna triplets further significantly increased the brightness and quantum yield of UCNPs. These findings have led to the design of dye-UCNP hybrids with upconverted emission of more than four orders of magnitude brighter than bare UCNPs. In 2017, the Kim group reported multi-dye-sensitized NaYF$_4$:Yb/Tm UCNPs with dramatically widened photo-absorption bandwidths by harnessing sequential energy transfer.[110] The absorption band of UCNPs spans from NIR to the entire visible range (Figure 6c), intensifying upconverted UV emission. Apart from excitation sensitization, commercially available ATTO-542 dye molecules were used to enhance Yb/Er-based nanoparticles via emission dye-sensitization.[111] The energy gap between the LUMO and HOMO of ATTO-542 matches perfectly dominant emitting transitions of Er^{3+}, enabling efficient energy transfer from Er^{3+} to the dye (Figure 6d). Owing to their much efficient radiative decay than Er^{3+}, ATTO-542-decorated UCNPs showed over 2-fold and 10-fold higher emission intensity than organic-soluble and water-soluble nanoparticles, respectively, accompanied by accelerated emission rates.

5. Recent Advances in Upconversion-Mediated Photocatalytic Applications

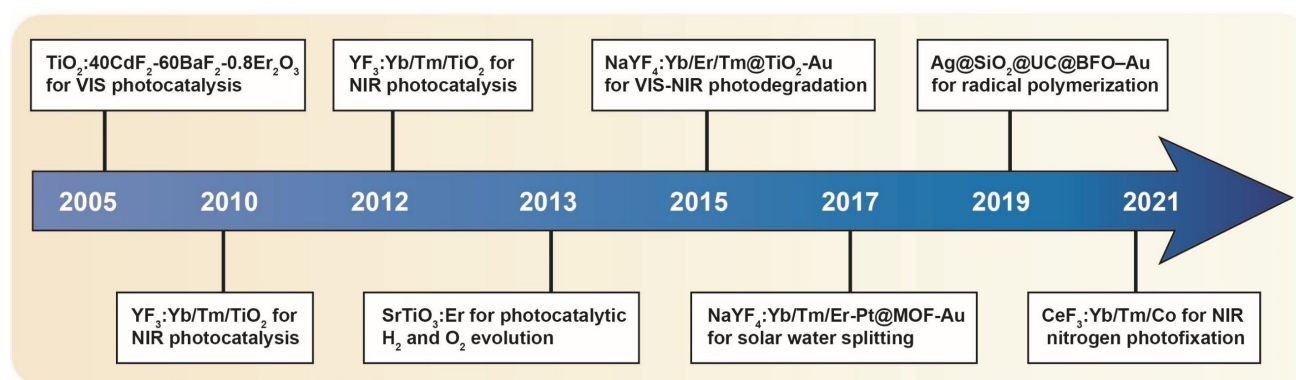Lanthanide-doped upconversion materials have shown great promise in enhancing the optical response of photocatalysts to a wide solar spectrum (Scheme 1). In this section, we review the critical role of lanthanide-doped UCNPs in harvesting NIR light for photocatalysis and environmental applications (Table 1).

5.1. Water Splitting

Photocatalytic water splitting is the most promising and renewable choice for hydrogen production. Numerous attempts have been made to enhance the photocatalytic activities of water splitting by incorporating lanthanides into photocatalysts; however, their photocatalytic systems are limited to light harvesting in the ultraviolet and visible region.[112] If the infrared spectrum could be harvested, the photocatalytic performance of those photocatalytic systems would be significantly boosted. As a case in point, Zhang et al. combined NaYF$_4$:Yb/Er UCNPs and W$_{18}$O$_{49}$ nanowires to form hierarchical heterostructures that promote photocatalytic hydrogen evolution.[113] These UCNP-based heterostructures selectively enhanced upconversion luminescence by two orders of magnitude via a localized surface plasmon resonance (LSPR) effect. The researchers argued that incident NIR photons are first converted to LSPR oscillation energy via W$_{18}$O$_{49}$ nanowires. LSPR oscillation energy is then transferred to neighboring NaYF$_4$:Yb/Er nanoparticles, significantly boosting upconversion luminescence due to the effects of plasmon-enhanced localized electric fields and photo-thermally enhanced electron population. The enhanced upconversion emission then re-excites the LSPR oscillation of W$_{18}$O$_{49}$ nanowires in the visible region, resulting in the LSPR-mediated selective absorption of upconversion luminescence. Surface plasmon-mediated energy upconversion improved photocatalytic hydrogen evolution from ammonia borane by 35-fold, making lanthanide-doped UCNPs promising for photocatalytic applications.

5.2. Water Treatment

The presence of suspended matter and organic contaminants in wastewater prevents UV/Vis light from penetrating wastewater, restricting the practical use of photocatalysts in wastewater

Scheme 1. Milestones in the development of lanthanide-doped upconversion materials for photocatalysis.

Table 1. Recent advances in upconversion-mediated photocatalytic applications.

Photocatalysts	Strategies	Synthesis	Absorption Range	Applications	Refs.
Water Splitting					
Integrated CdS with $Ln_{52}Ni_{56}$ clusters (Ln = Eu, Pr, Nd, and Gd)	VB potential engineering	One-step assembly via hydrothermal	Visible	Enhanced hydrogen evolution (up to 7.8 times more efficient than pristine CdS)	[112]
$NaYF_4$:Yb/Er UCNP-$W_{18}O_{49}$ nanowire heterostructures	Surface plasmon resonance	Solvothermal, hydrothermal, or self-assembly via solvent evaporation	Visible to near-infrared (plasmon-enhanced)	Enhanced hydrogen evolution (~3.5 times more efficient than pristine $W_{18}O_{49}$ nanowires)	[113]
Water Treatment					
Gd^{3+}-doped UCNP-TiO_2 composite	Doping and defect engineering	Solvothermal and surface growth	Ultraviolet to near-infrared	Enhanced degradation of rhodamine B (3 times more efficient than conventional UCNP-TiO_2 systems)	[114]
Tridoped β-$NaYF_4$:Yb/Tm/Gd upconversion nanorod-embedded TiO_2	VB potential engineering	Hydrothermal and spin coating	Ultraviolet to near-infrared	Enhanced degradation of nitrobenzene (1.66 times more efficient than pristine TiO_2)	[115]
$NaBiF_4$:Yb/Tm-Bi_2WO_6 composite	VB potential engineering	Hydrothermal	Ultraviolet to near-infrared	Enhanced degradation of rhodamine B	[116]
Nitrogen Photofixation					
Co-doped hollow CeF_3; Yb/Tm nanospheres	Doping and defect engineering	Microwave hydrothermal	Ultraviolet to near-infrared	Enhanced nitrogen reduction for nitrogen fixation (2.87 times more efficient than pristine CeF_3)	[117]
Photoelectrocatalytic Applications					
$NaYF_4$:Er/Yb-coupled Au-hematite nanorods	Surface plasmon resonance	Hydrothermal	Ultraviolet to near-infrared (plasmon-enhanced)	Enhanced water splitting (93 times more efficient than UCNPs alone)	[118]
Au nanoparticle-UCNP-TiO_2 hybrid nanostructures	Surface plasmon resonance	Solvothermal, dispersion, solvent evaporation	Ultraviolet to near-infrared (plasmon-enhanced)	Enhanced water splitting (up to 2.2 times more efficient than pristine TiO_2)	[119]

remediation. Developing photocatalysts that respond to NIR light may resolve this issue as NIR light allows great penetration depths. Wang et al. developed a NIR-responsive, UCNP-TiO$_2$ hybrid structure with surface adhesion capacity for organic chromophore decomposition in wastewater.[114] Besides captivating NIR light in water, incorporation of heavy Gd^{3+} on the surface of the photocatalysis system enhanced the photo-oxidation of organic contaminants and allowed selective cyclo-reversion of rhodamine B in place of conventional *N*-demethylation. In addition, Kwon et al. embedded β-NaYF$_4$:Yb/Tm/Gd upconversion nanorods on carbon-doped mesostructured TiO$_2$ for organic waste degradation.[115] Zhang et al. incorporated NaBiF$_4$:Yb/Tm UCNPs into semiconductor Bi$_2$WO$_6$ photocatalysts for pollutant degradation.[116] Excitingly, their designed hybrid photocatalyst enabled a rhodamine B degradation efficiency of 98% in 27 min under simulated light.

5.3. Nitrogen Photofixation

Photocatalytic reduction of nitrogen to ammonia is desirable as it serves as a potential alternative to the conventional, energy-intensive Haber-Bosch nitrogen fixation process. However, the photocatalysts used for nitrogen fixation suffer from low nitrogen adsorption, low activation energy, and high recombination rates of photogenerated charges. Zhong et al. doped hollow CeF$_3$ nanospheres with Yb^{3+} and Tm^{3+} to form hybrid catalysts.[117] Intriguingly, these catalysts achieved an NH$_4^+$ concentration up to 15.06 μmol/(g$_{cat}$h) under simulated sunlight and 6.22 μmol/(g$_{cat}$h) under NIR light. The hollow architecture of lanthanide-doped catalysts demonstrates strong capability of upconverting NIR light to ultraviolet and visible light.

5.4. Photoelectrocatalytic Applications

NaYF$_4$:Er/Yb UCNPs have been incorporated into conventional photoelectrode hematites for enhanced light trapping and absorption.[118] These UCNPs can upconvert photons from 980 nm to 510–570 nm within the bandgap of hematites. Incorporating a gold nanodisk array with a plasmonic peak centered at ~1000 nm into the photocatalytic system further enhanced photocurrent by 93-fold. Similarly, Boppella et al. also integrated upconversion nanocrystals and gold nanoparticles into TiO$_2$ inverse opal nanostructures for enhanced photo-electrochemical water splitting.[119] These hybrid nanostructures displayed a 10-fold enhancement in photocurrent density under UV-vis-NIR radiation than pristine TiO$_2$. These two studies present the potential of plasmonic effects in improving the upconversion efficiency of lanthanide-based photocatalytic systems.

6. Summary and Perspective

In summary, we have reviewed the essential design principles of photocatalytic semiconductors. An important emphasis is

placed on recent advances in enhancing the emission brightness of upconversion materials. Moreover, we have highlighted the latest advances in lanthanide-doped upconversion materials for photocatalytic applications. The integration of upconversion materials with semiconductors has proven effective in harvesting NIR light. However, despite the enticing prospects of UCNPs in broadening light absorption for photocatalysts, the practical implementation of UCNPs for photocatalysis is still hindered by several significant challenges, including low absorption capacity, narrow excitation band, and low conversion efficiency. Yb^{3+} and Nd^{3+} ions are regarded as the most efficient NIR light sensitizers. However, these two lanthanides have small dipole moments and low absorption coefficients, exhibiting two dominant narrow absorption bands centered at 980 nm and 808 nm, respectively. These constraints have imposed high-power laser excitation at specific wavelengths to achieve efficient upconversion.

Various strategies have been proposed to tackle the above-mentioned drawbacks. One increasingly appealing approach to improve light absorption is to couple UCNPs with quantum dots or organic molecules because of their superior optical properties. Recently, sensitization of UCNPs by singlet or triplet states of organic molecules has enhanced upconversion emission brightness by three orders of magnitude. Plasmonic or dielectric nanocavities capable of generating photonic hotspots with extremely high field intensity provide an excellent platform to accelerate upconversion processes. Coupling UCNPs to these nanoresonators represents another versatile and efficacious approach to significantly improving upconversion efficiency. Considering great diversity and wide optical tunability in plasmonic, dielectric, semiconducting nanomaterials and dye molecules, appropriate selection of components and rational manipulation of the energy flow between UCNPs and diverse photosensitizers or photonic nanocavities are expected to facilitate the construction of highly efficient upconversion nanosystems. On the other hand, core-shell engineering with a conformal coating of photocatalysts onto nanoparticle surfaces is particularly useful as it allows full utilization of upconversion emission by semiconductor photocatalysts. State-of-the-art gap-plasmon nanocavities are typically fabricated on planar substrates. Further development of water-dispersible photonic nanocavities is desirable for the implementation of UCNPs for photocatalysis in aqueous systems in which many photocatalytic reactions are carried out.

Acknowledgments

Conflict of Interest

The authors declare no conflict of interest.

[1] N. Serpone, A. V. Emeline, *J. Phys. Chem. Lett.* **2012**, *3*, 673.
[2] B. C. Hodges, E. L. Cates, J. H. Kim, *Nat. Nanotechnol.* **2018**, *13*, 642.
[3] L. Wang, J. Zhao, H. Liu, J. Huang, *J. Inst. Chem.* **2018**, *93*, 590.
[4] Q. Wang, K. Domen, *Chem. Rev.* **2020**, *120*, 919.
[5] P. Van Viet, C. M. Thi, L. Van Hieu, *J. Nanomater.* **2016**, *2016*, 117908.
[6] C. Cheng, B. Liu, H. Yang, W. Zhou, L. Sun, R. Chen, S. F. Yu, J. Zhang, H. Gong, H. Sun, H. J. Fan, *ACS Nano* **2009**, *3*, 3069.
[7] S. M. Gupta, M. Tripathi, *Chin. Sci. Bull.* **2011**, *56*, 1639.
[8] K. Nakata, A. Fujishima, *J. Photochem. Photobiol. C* **2012**, *13*, 169.
[9] S. Chen, T. Takata, K. Domen, *Nat. Rev. Mater.* **2017**, *2*, 17050.
[10] A. Kudo, Y. Miseki, *Chem. Soc. Rev.* **2009**, *38*, 253.
[11] T. Takata, K. Domen, *ACS Energy Lett.* **2019**, *4*, 542.
[12] B. Zhang, S. Cao, M. Du, X. Ye, Y. Wang, J. Ye, *Catalysts* **2019**, *9*, 91.
[13] J. Lu, W. Zhou, X. Zhang, G. Xiang, *J. Phys. Chem. Lett.* **2020**, *11*, 1038.
[14] W. W. Liu, R. F. Peng, *J. Electron. Sci. Technol.* **2020**, *18*, 100020.
[15] C. Tian, Q. Zhang, A. Wu, M. Jiang, B. Jiang, H. Fu, *Chem. Commun.* **2012**, *48*, 2858.
[16] D. Voiry, H. S. Shin, K. P. Loh, M. Chhowalla, *Nat. Chem. Rev.* **2018**, *2*, 0105.
[17] L. Cheng, Q. Xiang, Y. Liao, H. Zhang, *Energy Environ. Sci.* **2018**, *11*, 1362.
[18] M. Mishra, D. M. Chun, *Appl. Catal. A* **2015**, *498*, 126.
[19] J. Wen, J. Xie, X. Chen, L. Xin, *Appl. Surf. Sci.* **2016**, *391*, 72.
[20] Y. Wu, H. Zhang, J. Wang, J. Pan, X. Zhang, D. Wu, X. Zhang, J. Jie, *ACS Appl. Energy Mater.* **2020**, *3*, 8765.
[21] J. Cao, C. Zhou, H. Lin, B. Xu, S. Chen, *Appl. Surf. Sci.* **2013**, *284*, 263.
[22] H. Yan, X. Wang, M. Yao, X. Yao, *Prog. Nat. Sci. Mater. Int.* **2013**, *23*, 402.
[23] T. S. Atabaev, A. Molkenova, *Front. Mater.* **2019**, *13*, 335.
[24] M. Freitag, N. Möller, A. Rühling, C. A. Strassert, B. J. Ravoo, F. Glorius, *ChemPhotoChem* **2019**, *3*, 24.
[25] W. Gao, B. Tian, W. Zhang, X. Zhang, Y. Wu, G. Lu, *Appl. Catal. B* **2019**, *257*, 117908.
[26] Q. Zhang, F. Yang, Z. Xu, M. Chaker, D. Ma, *Nanoscale Horiz.* **2019**, *4*, 579.
[27] Q. Tian, W. Yao, W. Wu, C. Jiang, *Nanoscale Horiz.* **2019**, *4*, 10.
[28] M. Q. Yang, M. Gao, M. Hong, G. W. Ho, *Adv. Mater.* **2018**, *30*, 1802894.
[29] W. Yang, X. Li, D. Chi, H. Zhang, X. Liu, *Nanotechnology* **2014**, *25*, 482001.
[30] M.-Q. Yang, M. Gao, M. Hong, G. W. Ho, *Adv. Mater.* **2018**, *30*, 1802894.
[31] R. Asahi, T. Morikawa, H. Irie, T. Ohwaki, *Chem. Rev.* **2014**, *114*, 9824.
[32] M. R. D. Khaki, M. S. Shafeeyan, A. A. A. Raman, W. M. A. W. Daud, *J. Environ. Manage.* **2017**, *198*, 78.
[33] A. Khlyustova, N. Sirotkin, T. Kusova, A. Kraev, V. Titov, A. Agafonov, *Mater. Adv.* **2020**, *1*, 1193.
[34] R. Niishiro, H. Kato, A. Kudo, *Phys. Chem. Chem. Phys.* **2005**, *7*, 2241.
[35] T. Ishii, H. Kato, A. Kudo, *J. Photochem. Photobiol. A* **2004**, *163*, 181.
[36] X. Chen, S. Shen, L. Guo, S. S. Mao, *Chem. Rev.* **2010**, 110, 6503..
[37] Y. He, Q. Lei, C. Li, Y. Han, Z. Shi, S. Feng, *Mater. Today* **2021**, DOI: 10.1016/j.mattod.2021.03.021.
[38] J. Zheng, J. Lyu, R. Wang, C. Xie, H. Zhou, S. P. Jiang, S. Wang, *Nat. Commun.* **2018**, *9*, 3572.
[39] J. Wu, X. Li, W. Shi, P. Ling, Y. Sun, X. Jiao, S. Gao, L. Liang, J. Xu, W. Yan, C. Wang, Y. Xie, *Angew. Chem. Int. Ed.* **2018**, *57*, 8719.
[40] Y. He, H. Rao, K. Song, J. Li, Y. Yu, Y. Lou, C. Li, Y. Han, Z. Shi, S. Feng, *Adv. Funct. Mater.* **2019**, *29*, 1905153.
[41] H. Lin, P. A. Maggard, *Inorg. Chem.* **2008**, *47*, 8044.
[42] H. Lin, P. A. Maggard, *Inorg. Chem.* **2007**, *46*, 1283.
[43] O. Palasyuk, A. Palasyuk, P. A. Maggard, *J. Solid State Chem.* **2010**, *183*, 814.
[44] Y. Hosogi, Y. Shimodaira, H. Kato, H. Kobayashi, A. Kudo, *Chem. Mater.* **2008**, *20*, 1299.
[45] H. Suzuki, H. Kunioku, M. Higashi, O. Tomita, D. Kato, H. Kageyama, R. Abe, *Chem. Mater.* **2018**, *30*, 5862.
[46] J. Yoshimura, Y. Ebina, J. Kondo, K. Domen, A. Tanaka, *J. Phys. Chem.* **1993**, *97*, 1970.
[47] N. Arai, N. Saito, H. Nishiyama, Y. Shimodaira, H. Kobayashi, Y. Inoue, K. Sato, *Chem. Lett.* **2008**, *37*, 46.
[48] H. Nishiyama, H. Kobayashi, Y. Inoue, *ChemSusChem* **2011**, *4*, 208.
[49] H. Liu, J. Yuan, W. Shangguan, Y. Teraoka, *J. Phys. Chem. C* **2008**, *112*, 8521.
[50] K. Maeda, K. Teramura, D. Lu, T. Takata, N. Saito, Y. Inoue, K. Domen, *Nature* **2006**, *440*, 295.
[51] X. Zhang, T. Peng, S. Song, *J. Mater. Chem. A* **2016**, *4*, 2365.
[52] L. Wang, J. Shang, W. Hao, S. Jiang, S. Huang, T. Wang, Z. Sun, Y. Du, S. Dou, T. Xie, D. Wang, J. Wang, *Sci. Rep.* **2014**, *4*, 1.
[53] Y. Park, S. H. Lee, S. O. Kang, W. Choi, *Chem. Commun.* **2010**, *46*, 2477.
[54] N. Manfredi, M. Monai, T. Montini, F. Peri, F. De Angelis, P. Fornasiero, A. Abbotto, *ACS Energy Lett.* **2018**, *3*, 85.
[55] T. Torimoto, H. Horibe, T. Kameyama, K. I. Okazaki, S. Ikeda, M. Matsumura, A. Ishikawa, H. Ishihara, *J. Phys. Chem. Lett.* **2011**, *2*, 2057.
[56] Z. Zhang, A. Li, S. W. Cao, M. Bosman, S. Li, C. Xue, *Nanoscale* **2014**, *6*, 5217.
[57] W. Hou, S. B. Cronin, *Adv. Funct. Mater.* **2013**, *23*, 1612.
[58] L. Ma, S. J. Ding, D. J. Yang, *Dalton Trans.* **2018**, *47*, 16969.
[59] C. G. Silva, R. Juárez, T. Marino, R. Molinari, H. García, *J. Am. Chem. Soc.* **2011**, *133*, 595.
[60] H. Liu, J. Xu, H. Wang, Y. Liu, Q. Ruan, Y. Wu, X. Liu, J. K. W. Yang, *Adv. Mater.* **2019**, 31, 1807900.
[61] Q. Wang, T. Hisatomi, S. S. K. Ma, Y. Li, K. Domen, *Chem. Mater.* **2014**, *26*, 4144.
[62] X. She, J. Wu, H. Xu, J. Zhong, Y. Wang, Y. Song, K. Nie, Y. Liu, Y. Yang, M. T. F. Rodrigues, R. Vajtai, J. Lou, D. Du, H. Li, P. M. Ajayan, *Adv. Energy Mater.* **2017**, *7*, 1700025.
[63] Q. Wang, T. Hisatomi, Y. Suzuki, Z. Pan, J. Seo, M. Katayama, T. Minegishi, H. Nishiyama, T. Takata, K. Seki, A. Kudo, T. Yamada, K. Domen, *J. Am. Chem. Soc.* **2017**, *139*, 1675.
[64] H. Aouani, M. Rahmani, M. Navarro-Cía, S. A. Maier, *Nat. Nanotechnol.* **2014**, *9*, 290.
[65] S. H. C. Askes, S. Bonnet, *Nat. Chem. Rev.* **2018**, *2*, 437.
[66] K. Zheng, K. Y. Loh, Y. Wang, Q. Chen, J. Fan, T. Jung, S. H. Nam, Y. D. Suh, X. Liu, *Nano Today* **2019**, *29*, 100797.
[67] Y. Wu, M. J. Y. Ang, M. Sun, B. Huang, X. Liu, *J. Phys. D* **2019**, *52*, 383002.
[68] F. Wang, D. Banerjee, Y. Liu, X. Chen, X. Liu, *Analyst* **2010**, *135*, 1839.
[69] S. M. Borisov, C. Larndorfer, I. Klimant, *Adv. Funct. Mater.* **2012**, *22*, 4360.
[70] B. Chen, F. Wang, *Trends Chem.* **2020**, *2*, 427.
[71] X. Qin, J. Xu, Y. Wu, X. Liu, *ACS Cent. Sci.* **2019**, *5*, 29.
[72] Y. Wu, J. Xu, X. Qin, J. Xu, X. Liu, *Nat. Commun.* **2021**, *12*, 2022.
[73] S. Zha, H. F. Chau, W. Y. Chau, L. S. Chan, J. Lin, K. W. Lo, W. Chi-Shing Cho, Y. L. Yip, S. W. Tsao, P. J. Farrell, L. Feng, J. M. Di, G. L. Law, H. L. Lung, K. L. Wong, *Adv. Sci.* **2021**, *8*, 2002919.
[74] B. Ding, S. Shao, C. Yu, B. Teng, M. Wang, Z. Cheng, K. L. Wong, P. Ma, J. Lin, *Adv. Mater.* **2018**, *30*, 1802479.
[75] S. Zha, Y. H. Fung, H. F. Chau, P. Ma, J. Lin, J. Wang, L. S. Chan, G. Zhu, H. L. Lung, K. L. Wong, *Nanoscale* **2018**, *10*, 15632.
[76] S. Chen, A. Z. Weitemier, X. Zeng, L. He, X. Wang, Y. Tao, A. J. Y. Huang, Y. Hashimotodani, M. Kano, H. Iwasaki, L. K. Parajuli, S. Okabe, D. B. Loong Teh, A. H. All, I. Tsutsui-Kimura, K. F. Tanaka, X. Liu, T. J. McHugh, *Science* **2018**, *359*, 679.
[77] L. Liang, Z. Feng, Q. Zhang, T. Do Cong, Y. Wang, X. Qin, Z. Yi, M. J. Y. Ang, L. Zhou, H. Feng, B. Xing, M. Gu, X. Li, X. Liu, *Nat. Nanotechnol.* **2021**, doi.org/10.1038/s41565-021-00927-y.
[78] J. Zhou, S. Xu, J. Zhang, J. Qiu, *Nanoscale* **2015**, *7*, 15026.
[79] F. Wang, Y. Han, C. S. Lim, Y. Lu, J. Wang, J. Xu, H. Chen, C. Zhang, M. Hong, X. Liu, *Nature* **2010**, *463*, 1061.
[80] S. Wilhelm, *ACS Nano* **2017**, *11*, 10644.
[81] Q. Liu, Y. Zhang, C. S. Peng, T. Yang, L. M. Joubert, S. Chu, *Nat. Photonics* **2018**, *12*, 548.
[82] S. Wu, G. Han, D. J. Milliron, S. Aloni, V. Altoe, D. V. Talapin, B. E. Cohen, P. J. Schuck, *Proc. Natl. Acad. Sci. USA* **2009**, *106*, 10917.
[83] S. Han, R. Deng, X. Xie, X. Liu, *Angew. Chem. Int. Ed.* **2014**, *53*, 11702.
[84] C. Renero-Lecuna, R. Martín-Rodríguez, R. Valiente, J. González, F. Rodríguez, K. W. Krämer, H. U. Güdel, *Chem. Mater.* **2011**, *23*, 3442.
[85] C. Zhao, X. Kong, X. Liu, L. Tu, F. Wu, Y. Zhang, K. Liu, Q. Zeng, H. Zhang, *Nanoscale* **2013**, *5*, 8084.
[86] H. Liang, Y. Zheng, G. Chen, L. Wu, Z. Zhang, W. Cao, *J. Alloys Compd.* **2011**, *509*, 409.

[87] L. Jiang, S. Xiao, X. Yang, J. Ding, K. Dong, *Appl. Phys. B* **2012**, *107*, 477.

[88] Y. Zhang, Y. Shen, M. Liu, Y. Han, X. Mo, R. Jiang, Z. Lei, Z. Liu, F. Shi, W. Qin, *CrystEngComm* **2017**, *19*, 1304.

[89] Q. Huang, J. Yu, E. Ma, K. Lin, *J. Phys. Chem. C* **2010**, *114*, 4719.

[90] S. Wen, J. Zhou, K. Zheng, A. Bednarkiewicz, X. Liu, D. Jin, *Nat. Commun.* **2018**, *9*, 2415.

[91] J. Wang, R. Deng, M. A. Macdonald, B. Chen, J. Yuan, F. Wang, D. Chi, T. S. Andy Hor, P. Zhang, G. Liu, Y. Han, X. Liu, *Nat. Mater.* **2014**, *13*, 157.

[92] B. Zhou, B. Tang, C. Zhang, C. Qin, Z. Gu, Y. Ma, T. Zhai, J. Yao, *Nat. Commun.* **2020**, *11*, 1174.

[93] F. Wang, J. Wang, X. Liu, *Angew. Chem. Int. Ed.* **2010**, *49*, 7456.

[94] Q. Su, S. Han, X. Xie, H. Zhu, H. Chen, C. K. Chen, R. S. Liu, X. Chen, F. Wang, X. Liu, *J. Am. Chem. Soc.* **2012**, *134*, 20849.

[95] H. Qiu, C. Yang, W. Shao, J. Damasco, X. Wang, H. Ågren, P. Prasad, G. Chen, *Nanomaterials* **2014**, *4*, 55.

[96] X. Qin, A. N. Carneiro Neto, R. L. Longo, Y. Wu, O. L. Malta, X. Liu, *J. Phys. Chem. Lett.* **2021**, *12*, 1520.

[97] V. A. G. Rivera, F. A. Ferri, E. Marega, *Plasmonics-Principles and Applications* **2012**, 283–312.

[98] J. J. Baumberg, J. Aizpurua, M. H. Mikkelsen, D. R. Smith, *Nat. Mater.* **2019**, *18*, 668.

[99] Y. Wu, J. Xu, E. T. Poh, L. Liang, H. Liu, J. K. W. Yang, C. W. Qiu, R. A. L. Vallée, X. Liu, *Nat. Nanotechnol.* **2019**, *14*, 1110.

[100] X. Wu, Z. Dong, M. Asbahi, Y. Wu, H. Wang, L. Liang, R. J. H. Ng, H. Liu, R. A. L. Vallée, J. K. W. Yang, X. Liu, *Nano Lett.* **2021**, *21*, 3044.

[101] S. Wu, H. Xia, J. Xu, X. Sun, X. Liu, *Adv. Mater.* **2018**, *30*, 1803362.

[102] M. Wu, S. T. Ha, S. Shendre, E. G. Durmusoglu, W. K. Koh, D. R. Abujetas, J. A. Sánchez-Gil, R. Paniagua-Domínguez, H. V. Demir, A. I. Kuznetsov, *Nano Lett.* **2020**, *20*, 6005.

[103] L. Liang, D. B. L. Teh, N. D. Dinh, W. Chen, Q. Chen, Y. Wu, S. Chowdhury, A. Yamanaka, T. C. Sum, C. H. Chen, N. V. Thakor, A. H. All, X. Liu, *Nat. Commun.* **2019**, *10*, 1391.

[104] T. Sun, Y. Li, W. L. Ho, Q. Zhu, X. Chen, L. Jin, H. Zhu, B. Huang, J. Lin, B. E. Little, S. T. Chu, F. Wang, *Nat. Commun.* **2019**, *10*, 1811.

[105] X. Xie, Z. Li, Y. Zhang, S. Guo, A. I. Pendharkar, M. Lu, L. Huang, W. Huang, G. Han, *Small* **2017**, *13*, 1602843.

[106] S. Han, R. Deng, Q. Gu, L. Ni, U. Huynh, J. Zhang, Z. Yi, B. Zhao, H. Tamura, A. Pershin, H. Xu, Z. Huang, S. Ahmad, M. Abdi-Jalebi, A. Sadhanala, M. L. Tang, A. Bakulin, D. Beljonne, X. Liu, A. Rao, *Nature* **2020**, *587*, 594.

[107] R. Marin, D. Jaque, A. Benayas, *Nanoscale Horiz.* **2021**, *6*, 209.

[108] G. Chen, J. Damasco, H. Qiu, W. Shao, T. Y. Ohulchanskyy, R. R. Valiev, X. Wu, G. Han, Y. Wang, C. Yang, H. Ågren, P. N. Prasad, *Nano Lett.* **2015**, *15*, 7400.

[109] D. J. Garfield, N. J. Borys, S. M. Hamed, N. A. Torquato, C. A. Tajon, B. Tian, B. Shevitski, E. S. Barnard, Y. D. Suh, S. Aloni, J. B. Neaton, E. M. Chan, B. E. Cohen, P. J. Schuck, *Nat. Photonics* **2018**, *12*, 402.

[110] J. Lee, B. Yoo, H. Lee, G. D. Cha, H. S. Lee, Y. Cho, S. Y. Kim, H. Seo, W. Lee, D. Son, M. Kang, H. M. Kim, Y. I. Park, T. Hyeon, D. H. Kim, *Adv. Mater.* **2017**, *29*, 1603169.

[111] M. D. Wisser, S. Fischer, C. Siefe, A. P. Alivisatos, A. Salleo, J. A. Dionne, *Nano Lett.* **2018**, *18*, 2689.

[112] R. Chen, Z. H. Yan, X. J. Kong, L. S. Long, L. S. Zheng, *Angew. Chem. Int. Ed.* **2018**, *57*, 16796.

[113] Z. Zhang, Y. Liu, Y. Fang, B. Cao, J. Huang, K. Liu, B. Dong, *Adv. Sci.* **2018**, *5*, 1800748.

[114] J. Wang, H. Wang, S. Zuo, X. Jin, B. Zheng, R. Deng, W. Liu, J. Wang, *Environ. Sci.-Nano* **2020**, *7*, 3333.

[115] H. Kwon, F. Marques Mota, K. Chung, Y. J. Jang, J. K. Hyun, J. Lee, D. H. Kim, *ACS Sustainable Chem. Eng.* **2018**, *6*, 1310.

[116] C. Zhang, Z. Fu, F. Hong, J. Dou, T. Dong, Y. Zhang, D. Li, G. Liu, X. Dong, J. Wang, *J. Solid State Chem.* **2021**, *300*, 122248.

[117] M. Zhong, Z. Wang, D. Dai, B. Yang, S. Zuo, C. Yao, F. Wu, X. Li, *J. Rare Earth* **2021**, DOI 10.1016/j.jre.2021.03.004.

[118] Q. Jiang, X. Xie, D. J. Riley, F. Xie, *J. Chem. Phys.* **2020**, *153*, 011102.

[119] R. Boppella, F. Marques Mota, J. W. Lim, S. T. Kochuveedu, S. Ahn, J. Lee, D. Kawaguchi, K. Tanaka, D. H. Kim, *ACS Appl. Mater. Interfaces* **2019**, *2*, 3780.